

Fractional modelling of the reverse osmosis process used for dam water desalination

Abouda L.¹, Azizi A.^{2*}, Hanini S.¹, Moussaoui M.³, Cherifi H.¹ and Laidi M.¹

¹University of Yahia Fares, Faculty of Technology, Department of Process Engineering and Environment, Urban hub, Medea, Algeria

²University of Amar Telidji, Faculty of Technology, Department of The Common Trunk Sciences and Technology, Highway Ghardaia post box G37 (M'kam) 03000, Laghouat, Algeria

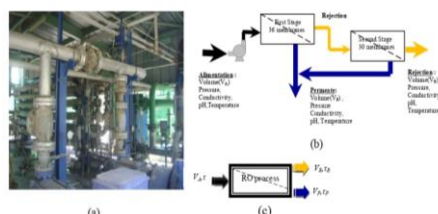
³University of Bouira, Bouira, Algeria

Received: 09/06/2023, Accepted: 27/07/2023, Available online: 12/08/2023

*to whom all correspondence should be addressed: e-mail: a.azizi@lagh-univ.dz

<https://doi.org/10.30955/gnj.005186>

Graphical abstract



The RO desalination process (a): Picture; (b): block flow diagram (c): Fractional modelling inputs and outputs to monitor the performance of the RO process.

Abstract

This paper deals with new fractional models to follow the performance of a dam water reverse osmosis (DWRO) desalination system using the dimensionless cumulative volume of alimentation, permeate and rejection. The experimental data consist of 2561 points collected over 4 years period from 66 organics reverse osmosis (RO) membranes. The accuracy of the established fractional models was verified using statistical criteria and a comparison with ordinary models. The fractional dimensionless models (FDM) with optimal kinetic constants provided an accurate result and perfect consistency with the experimental data. As such, the coefficient of determination (R^2) values were 0.9975, 0.9750 and 0.9801, with lower average absolute relative deviation (AARD) around 8.03, 0.53 and 0.45, through lower root mean squared error (RMSE) about 1.452, 0.976 and 0.880 for alimentation, permeate and rejection, respectively.

Keywords: Fractional modelling, dimensionless parameters, kinetic separation, desalination, reverse osmosis

1. Introduction

The reverse osmosis (RO) process is considered one of the most important desalination technologies due to its

advantages, including flexibility, high efficiency and ease of operation (Feria-Díaz *et al.*, 2021). It can be used to produce drinking water and process water for various industrial applications, such as food and pharmaceutical. Since its invention in the 1950s (Glaser, 1998), the RO process has been extensively studied to enhance its development (Abid *et al.*, 2012; Dimitriou *et al.*, 2017; Alsarayreh *et al.*, 2020). Monitoring the performance of RO process is necessary to identify early symptoms of failure in order to improve maintenance and extend the process lifetime. However, one of the major limitations to adequately ensure its performance monitoring is the matter accumulation on the membrane, such as concentration polarization and fouling. This limitation gets hard the supervision of the RO membrane's performances and the involvement of multiple parameters in the separation process. This deficiency can be attributed to its enormous complexity leading to the uncertainties of the operating parameters (flow rate, pressure ...etc.).

Mathematical modelling has been widely employed to accurately describe the performance of the RO process. Developing an appropriate mathematical model that accounts the fouling is essential for optimizing design and improving efficiency, thus reducing the overall costs. However, the majority of previous modelling studies (Ruth *et al.*, 1933; Hermans and Bredée, 1935; Ho and Zydney, 2000; Jamal *et al.*, 2004 ; Fouladitajar *et al.*, 2013; Tien *et al.*, 2014; Heidari *et al.*, 2017; Goldrick *et al.*, 2017; Debnath *et al.*, 2019; Tong *et al.*, 2020; Xu *et al.*, 2020; Heidari *et al.*, 2021; Azizi *et al.*, 2022; Bchiti *et al.*, 2022) have relied on a limited range of experimental data, thus limiting their range of validity. On the other hand, the classical models cannot best represent all the phenomena that occur during the membrane separation process, unlike fractional models that have proven their performance for other processes (Kashchenko and Nikitin, 2014; Zhai *et al.*, 2015; Padrino, 2017; Obembe *et al.*, 2018; Kumar *et al.*, 2019; Ramírez *et al.*, 2017; De Souza Matias *et al.*, 2019; Lemus-Mondaca *et al.*, 2021; Mahdad *et al.*, 2021a; Mahdad *et al.*, 2021b; Friesen *et al.*, 2015;

Nikan *et al.*, 2020; Mirza *et al.*, 2021; El-Gazar *et al.*, 2021).

In this paper, new fractional dimensionless models (FDM) have been proposed to follow the performance of the DWRO desalination process using the dimensionless cumulative volumes of alimentation, permeate, and rejection. The proposed models were mathematically developed from the pseudo nth order (PNO) equation and resolved by the establishment of a software program. The FDMs were thoroughly tested using statistical criteria to assess their accuracy in representing the 2561 cumulative volumes of experimental data collected over the 4-year lifetime of the RO membranes.

2. Materials and methods

2.1. Description of water treatment by the ro process

The DWRO process was carried out at the antibiotic complex of Medea (North Algeria) for the production of ultra-pure water. The water stream, coming from the pre-treatment unit, is processed in the RO plant operating according to the scheme illustrated in Figure 1. The RO plant comprises eleven modules, each containing six membranes. They are arranged in two consecutive stages, where the first one includes six modules and the second consists of five modules. Each pressure vessel of the DWRO plant contains a spiral wound polyamide membrane. The technical specifications of the studied RO unit are summarized in Table 1.

Table 1. Technical specifications of the RO desalination process

Specification	Parameter	Value
Membrane	Membrane type	ROGA® - HR 8.5" "spirale"
	Number of modules (-)	11
	Number of membranes (-)	66
	Total surface area (m ²)	38.6
	Efficiency (%)	75
	Total treated water flow (m ³ .h ⁻¹)	92
	Permeate flow (m ³ h ⁻¹)	69
Alimentation	TDS (mg.L ⁻¹)	1960 –30120
	Salinity (%)	≤1.3
	Turbidity (JTU)	≤0.19
	Total hardness (mg. L ⁻¹)	≤1100
Operating conditions	Operating pressure (Bars)	35– 41
	Operating temperature (°C)	20 – 40
	Operating pH (-)	4 – 6

Table 2. Chemical cleaning cycles of the RO membranes

Cleaning cycle	1	2	3	4	5	6	7	8	9	10	11
t (h)	3126	3414	3798	3942	4086	4566	5262	5766	6438	6606	6966
τ (-)	0.09	0.10	0.11	0.11	0.11	0.13	0.15	0.16	0.18	0.18	0.19
Cleaning cycle	12	13	14	15	16	17	18	19	20	21	22
t (h)	11142	11382	11526	11838	11886	11982	12462	12822	13182	13734	15534
τ (-)	0.31	0.32	0.32	0.33	0.33	0.33	0.35	0.36	0.37	0.38	0.43

2.2. Fractional modelling

2.2.1. Model approach

The fractional models, established in this study for the RO process, were developed from the PNO equation that was originally proposed for expressing solid-liquid adsorption

The experimental data were collected at the alimentation, permeate and rejection of the RO unit every 2 hours over a span of 4 years covering the lifespan of the RO membranes. Throughout the monitoring period, the RO membranes were not replaced but underwent 22 chemical cleaning operations, whose cleaning periods are presented in Table 2.



Figure 1. The RO desalination process (a) Picture; (b) block flow diagram (c) Fractional modeling inputs and outputs to follow the performance of the RO process

(Lagergren, 1898; Blanchard *et al.*, 1984; Morais *et al.*, 2007; Özer, 2007; Morais *et al.*, 2008; Leyva-Ramos *et al.*, 2010; Tseng *et al.*, 2014). This adsorption mechanism is considered one of the mechanisms leading to RO membranes fouling and, consequently, to the reduction of permeate flow (Lee and Elimelech, 2006; Fritzmann *et al.*,

2007; Qrenawi and Abuhabib, 2020; Ahmed *et al.*, 2023). It is assumed that, during the flow of solute-rich water through an RO membrane, a portion of this solute will be adsorbed on the membrane, while the remaining portion will be removed. The adsorption kinetics of the solute can be expressed by equation (1):

$$\frac{dq(t)}{dt} = k'_n (q_{\max} - q_t)^n \quad (1)$$

Where $q(t)$ is the adsorbed amount of solute per unit mass of the membrane (mg g⁻¹); q_{\max} is the maximum adsorption capacity of the membrane per unit mass of the membrane (mg g⁻¹); t is the filtration time (h); k'_n is the rate constant of adsorption reaction of the PNO equation ((mg g⁻¹)¹⁻ⁿh⁻¹); n is the order of adsorption reaction (-).

On the other hand, membrane fouling can be characterized by the retention rate (γ) which represents the ratio between the adsorbed mass (m_{ad}) and the initial mass (m_{in}) of solute. It can be expressed according to equation (2):

$$\gamma = \frac{m_{ad}}{m_{in}} \quad (2)$$

The m_{ad} and m_{in} can be expressed by equation (3) and equation (4), respectively:

$$m_{ad} = q(t) \cdot M \quad (3)$$

$$m_{in} = v(t) \cdot C_{in} \quad (4)$$

Where C_{in} is the initial mass concentration of solute in the feed suspension (mg L⁻¹); M is the mass of RO membrane (g); $v(t)$ is the cumulative volume of the filtrate (m³).

By replacing equation (3) and equation (4) in equation (2), the adsorbed amount of solute can be expressed according to the equation (5):

$$q(t) = \frac{\gamma \cdot v(t) \cdot C_{in}}{M} \quad (5)$$

By replacing equation (5) in equation (1) and simplification, we obtain the equation (6):

$$\frac{dv(t)}{dt} = k'_n \left(\frac{\gamma \cdot C_{in}}{M} \right)^{n-1} (v_m - v(t))^n \quad (6)$$

Assuming that $K_n = k'_n \left(\frac{\gamma \cdot C_{in}}{M} \right)^{n-1}$, the equation (6) can be written as the equation (7) (Adda *et al.*, 2020; Mesli *et al.*, 2022):

$$\left. \begin{aligned} \frac{dv(t)}{dt} &= K_n (v_m - v(t))^n \\ v_{t=0} &= v(0) = 0 \end{aligned} \right\} \quad (7)$$

Where K_n is the rate constant of filtration of the O-PNO equation (L¹⁻ⁿ h⁻¹), v_m is the maximum cumulative volume of the filtrate (m³);

2.2.2. Solution of the differential equation

The differential equation (7), which expresses the variation of cumulative volume, has been resolved using ordinary and fractional methods (Caputo derivative, Laplace Transform) for the different order of n (0, 1, 2 and n). An example is presented below for the pseudo-zero order kinetics ($n=0$), which the equation (7) can be expressed by the equation (8):

$$\left. \begin{aligned} \frac{dv(t)}{dt} &= K_0 \\ v(0) &= 0 \end{aligned} \right\} \quad (8)$$

Where K_0 is the rate constant of filtration of the O-PZO equation (L h⁻¹).

Adopting the ordinary solution, the equation (8) can be expressed as the equation (9):

$$\int_0^{v_t} dv(t) = K_0 dt \quad (9)$$

By integration of equation (9) we get the equation (10):

$$v(t) = K_0 \cdot t \quad (10)$$

Adopting the fractional solution, the equation (8) can be expressed as the equation (11):

$$\left. \begin{aligned} {}_0 D_t^\alpha v(t) &= K_{0f} \\ v(0) &= 0 \end{aligned} \right\} \quad (11)$$

Using Laplace's direct and reverse transformation, equation (11) can be expressed as equation (12):

$$v(t) = \frac{K_{0f} \cdot t^\alpha}{\Gamma(\alpha + 1)} \quad (12)$$

Where K_{0f} is the rate constant of filtration of the F-PZO equation (L h^{-α}); α is the fractional order of time (-); Γ is the Gamma function.

The same procedure is applied to resolve the deferential equation (7) for the others pseudo-orders kinetic (1, 2 and n). The ordinary and fractional dimensional models are presented in the Table 3.

Table 3. The Ordinary and fractional dimensional models developed in this work

Solution type	Pseudo Order	Formula	Equation
ODE	0	$v(t) = K_0 \cdot t$	(13)
	1	$v(t) = v_m (1 - e^{-K_1 t})$	(14)
	2	$v(t) = \frac{t}{1 + v_m \cdot K_2 \cdot t}$	(15)

FDE	n	$v(t) = v_m \left[1 - \frac{1}{\left[\left((n-1) v_m^{n-1} \cdot K_n t \right)^{\frac{1}{n-1}} \right]} \right]$	(16)
	0	$v(t) = \frac{K_{0f} t^\alpha}{\Gamma(\alpha+1)}$	(17)
	1	$v(t) = v_m \left[1 - \sum_{n=0}^{\infty} \frac{(-1)^n \cdot K_{1f}^n t^{\alpha \cdot n}}{\Gamma(\alpha \cdot n + 1)} \right]$	(18)
	2	$v(t) = v_m \left[1 - \frac{\Gamma(\alpha+1)}{\Gamma(\alpha+1) + v_m \cdot K_{2f} t^\alpha} \right]$	(19)
	n	$v(t) = v_m \left[1 - \left[\frac{\Gamma(\alpha+1)}{\Gamma(\alpha+1) + (n-1) v_m^{n-1} \cdot K_{nf} t^\alpha} \right]^{\frac{1}{n-1}} \right]$	(20)

Where K_1 is the rate constant of filtration of the O-PFO equation (h^{-1}); K_{1f} is the rate constant of filtration of the F-PFO equation ($\text{h}^{-\alpha}$); K_2 is the rate constant of filtration of the O-PSO equation ($\text{L}^{-1} \text{h}^{-1}$); K_{2f} is the rate constant of filtration of the F-PSO equation ($\text{L}^{-1} \text{h}^{-\alpha}$); K_{nf} is the rate constant of filtration of the F-PNO equation ($\text{L}^{1-n} \text{h}^{-\alpha}$).

2.2.3. Transformation to dimensionless models

There are several significant advantages to describe the RO process using dimensionless models, including: simplify the parametric representation, reducing the number of variables and enabling cross-scales experiments. The dimensional models, presented in Table 3, were transformed to dimensionless models according to the equations (21) and (22), respectively:

$$V = \frac{v(t)}{v_m} \quad (21)$$

$$\tau = \frac{t}{t_m} \quad (22)$$

Where V is the dimensionless cumulative volume of the filtrate (-); τ is the dimensionless filtration time (-); t_m is the maximum filtration time (h).

An example of the transformation to a dimensionless model is presented below for the pseudo-zero order

kinetics ($n=0$). By replacing the equations (21) and (22) in the equation (13), we obtain the equation (23):

$$V \cdot v_m = K_0 \cdot t_m \cdot \tau \quad (23)$$

Assuming that $K_0 \cdot \frac{t_m}{v_m} = k_0$, the equation (23) can be written as the equation (24):

$$V = k_0 \cdot \tau \quad (24)$$

The same steps are followed to make the transformation to dimensionless models for the others pseudo-orders kinetic (1, 2 and n). The ordinary dimensionless models (ODM) and the fractional dimensionless models (FDM) are presented in Table 4.

Where k_n , k_0 , k_1 , k_2 are the constants of ordinary dimensionless models for n , 0, 1 and 2 order, respectively (-); k_{nf} , k_{0f} , k_{1f} , k_{2f} are the constant of fractional dimensionless models for n , 0, 1 and 2 order, respectively (-).

The transformation of experimental values of $v(t)$ and t to dimensionless values were achieved by relating them to the maximum experimental value v_m and t_m , respectively. The maximum experimental values are presented by Table 5.

Table 4. The ordinary and fractional dimensionless models developed in this work.

Classification	Model code	Formula	Equation
ODM	0	$V = k_0 \cdot \tau$	(24)
	1	$V = 1 - \text{Exp}(-k_1 \cdot \tau)$	(25)
	2	$V = \frac{1 + (k_2 - 1) \cdot \tau}{1 + k_2 \cdot \tau}$	(26)
	n	$V = 1 - \left[\frac{1}{1 + (n-1) \cdot k_n \cdot \tau} \right]^{\frac{1}{n-1}}$	(27)
FDM	0	$V = \frac{k_{0f}}{\Gamma(\alpha+1)} \cdot \tau^\alpha$	(28)
	1	$V = 1 - \text{Exp}(-k_{1f} \cdot \tau^\alpha)$	(29)

2	F-PSO	$V = \frac{k_{2,f} \cdot \tau^\alpha}{\Gamma(\alpha + 1) + k_{2,f} \cdot \tau^\alpha} \quad (30)$	
n	F-PNO	$V = 1 - \left[\frac{\Gamma(\alpha + 1)}{\Gamma(\alpha + 1) + (n - 1)k_{n,f} \cdot \tau^\alpha} \right]^{\frac{1}{n-1}} \quad (31)$	

Table 5. Maximum experimental values of cumulative volume and filtration time

Parameter	Alimentation	Permeate	Rejection
$v_m (10^{+3} \cdot m^3)$	3603.78	2144.07	1496.72
$t_m (10^{+3} \cdot m^3)$	36.37	36.37	36.37

2.3. Solving of the dimensionless models

The resolution of the developed ODM (equation (24) to (27)) and FDM (equation (28) to (31)), presented in Table 4, and the determination of its optimal kinetic constants (n , α , k_n and k_{nf}) have been conducted by setting up an establishment a MATLAB software program.

2.4. Evaluation of the models accuracy by statistical criteria

The applied models accuracy was assessed by the statistical criteria which quantify the error between the model results and the experimental values. The statistical criteria, used in this work, include the root mean squared error (RMSE) (Adda *et al.*, 2020), the average absolute relative deviation (AARD) (Jouyban *et al.*, 2002), the coefficient of determination (R^2) (Soleimani *et al.*, 2018), the mean absolute error (MAE) (Soleimani *et al.*, 2018), the sum of squares regression (SSR) (Coker, 1995) and the sum of squares error (SSE) (Coker, 1995), as follows:

$$RMSE = \sqrt{\frac{\sum_{i=1}^N (y_{i,exp} - y_{i,cal})^2}{N}} \quad (32)$$

$$AARD = \frac{1}{N - Z} \sum_{i=1}^n \left(\frac{y_{i,cal} - y_{i,exp}}{y_{i,exp}} \right) \times 100\% \quad (33)$$

$$R^2 = 1 - \frac{\sum_{i=1}^N (y_{i,exp} - y_{i,cal})^2}{\sum_{i=1}^N (y_{i,exp} - \bar{y})^2} \quad (34)$$

$$MAE = \frac{1}{n} \sum_{i=1}^n |y_{i,exp} - y_{i,cal}| \quad (35)$$

$$SSR = \sum_{i=1}^N (y_{i,cal} - \bar{y})^2 \quad (36)$$

$$SSE = \sum_{i=1}^N (y_{i,exp} - y_{i,cal})^2 \quad (37)$$

3. Results and discussion

3.1. Models' reliability and accuracy

The model's reliability and accuracy present the deadliest step in this study using the statistical criteria and the ability of the model's regression. In order, the statistical

criteria and the kinetic constants of the developed ODM and FDM are shown in Tables 6, 7 and Figure 2.

Based on the results presented in Table 6, it is evident that the fractional dimensionless models (F-PNO) gave the best values of statistical criteria, compared to the other tested models. This accuracy can be reflected with perfect R^2 (0.9975, 0.9750, 0.9801) and with lowers AARD (8.03, 0.53, 0.45), RMSE (1.452, 0.976, 0.880) and MAE (50.0109, 0.0032, 0.0026) for the alimentation, permeate and rejection, respectively.

The kinetic constants (Table 7) of fractional models (F-PNO) gave the following values of n (0.15, 1.59, 1.50), α (2.1693, 1.0425, 0.9206) and k_{nf} (2.74, 92.28, 50.94) for alimentation, permeate and rejection, respectively.

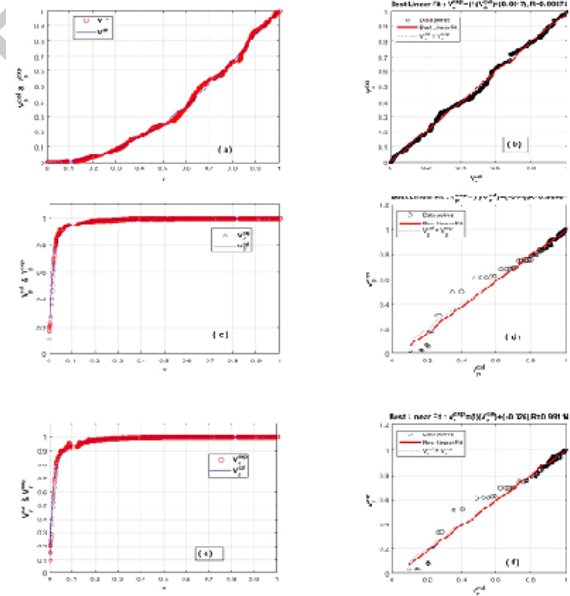


Figure 2. Scatter plot of the calculated values, by the F-PNO, versus the experimental values of dimensionless cumulative volume: for alimentation (a, b), permeate (c, d) and rejection (e, f)

Figure 2 argue the previous results, such as the scatter plot of the calculated values, by the fractional models (F-PNO), versus the experimental values of the dimensionless cumulative volume for alimentation (a, b), permeate (c, d) and rejection (e, f) were established the best regression.

Table 6. The statistical criteria of ODM and FDM for the dimensionless cumulative volume of alimentation, permeate and rejection

Classification		Statistical criteria					
		R^2	RMSE	AARD	MAE	SSR	SSE
Alimentation	O-PZO	0.8305	11.907	418.57	0.1062	218.961	36.297
	O-PFO	0.7074	15.646	527.31	0.1364	216.336	62.670
	O-PSO	-5.4171	73.269	2.9E5	0.6728	1371.128	1374.289
	O-PNO	0.8284	11.978	413.73	0.1064	217.853	36.729
	F-PZO	0.9968	1.619	13.96	0.0121	214.165	0.671
	F-PFO	0.9894	2.976	19.21	0.0242	214.310	2.267
	F-PSO	0.9739	4.668	30.56	0.0385	214.741	5.578
	F-PNO	0.9975	1.452	8.03	0.0109	214.158	0.540
Permeate	O-PZO	-45.914	42.341	36.78	0.3551	99.730	458.939
	O-PFO	0.9395	1.520	1.20	0.0096	9.945	0.591
	O-PSO	-0.0456	6.321	2.94	0.0131	10.140	10.229
	O-PNO	0.9309	1.624	0.62	0.0035	9.783	0.676
	F-PZO	0.48929	4.418	3.35	0.0232	9.782	4.996
	F-PFO	0.96447	1.16	0.88	0.0072	9.850	0.348
	F-PSO	0.9698	1.07	0.58	0.0035	9.799	0.295
	F-PNO	0.9750	0.976	0.53	0.0032	9.786	0.244
Rejection	O-PZO	-44.520	42.139	36.75	0.3538	99.072	454.584
	O-PFO	0.9280	1.675	1.28	0.0103	10.174	0.719
	O-PSO	-0.0524	6.408	3.13	0.0144	10.425	10.510
	O-PNO	0.9671	1.133	0.62	0.0040	9.997	0.328
	F-PZO	0.5212	4.322	3.34	0.0230	9.986	4.781
	F-PFO	0.9705	1.072	0.78	0.0064	10.034	0.294
	F-PSO	0.9718	1.047	0.73	0.0049	10.026	0.281
	F-PNO	0.9801	0.880	0.45	0.0026	9.998	0.198

3.2. Comparison between the fractional dimensionless models and others models

A comparison was established between the proposed fractional models (F-PNO) and other models in the literature (Table 8) according to the statistical criteria, the number of data points and the number of compartments of the studied process.

Such as, the proposed fractional models (F-PNO) provide an accurate result and a perfect consistency to the experimental data, against the literature models, with an excellent R^2 values (0.9975, 0.9750, and 0.9801) and with lowers AARD, RMSE, SSR and SSE for the three compartments of DWRO process: alimentation, permeate and rejection, respectively.

Table 7. The kinetic constants of ODM and FDM for the dimensionless cumulative volume of alimentation, permeate and rejection

Classification		Kinetic constants								
		$n(-)$	$\alpha (-)$	$k_0(-)$	$k_1(-)$	$k_2(-)$	$k_n(-)$	$k_{0f}(-)$	$k_{1f}(-)$	$k_{2f}(-)$
Alimentation	O-PZO	0	---	0.75	---	---	---	---	---	---
	O-PFO	1	---	---	0.96	---	---	---	---	---
	O-PSO	2	---	---	---	-	---	---	---	---
						43.001				
	O-PNO	0.18	---	---	---	---	0.78	---	---	---
	F-PZO	0	2.0132	---	---	---	---	2.10	---	---
	F-PFO	1	3.0352	---	---	---	---	---	2.31	---
	F-PSO	2	4.1253	---	---	---	---	---	---	1.62E2

Permeate	F-PNO	0.15	2.1693	---	---	---	---	---	---	---	2.74
	O-PZO	0	---	1.53	---	---	---	---	---	---	
	O-PFO	1	---	---	46.90	---	---	---	---	---	
	O-PSO	2	---	---	---	181.69	---	---	---	---	
	O-PNO	1.84	---	---	---	---	148.24	---	---	---	
	F-PZO	0	0.0551	---	---	---	---	0.9998	---	---	
	F-PFO	1	0.6443	---	---	---	---	---	13.52	---	
	F-PSO	2	1.2883	---	---	---	---	---	---	3.74E2	
	F-PNO	1.59	1.0425	---	---	---	---	---	---	92.28	
Rejection	O-PZO	0	---	1.54	---	---	---	---	---	---	
	O-PFO	1	---	---	44.92	---	---	---	---	---	
	O-PSO	2	---	---	---	190.74	---	---	---	---	
	O-PNO	1.79	---	---	---	---	107.15	---	---	---	
	F-PZO	0	0.0577	---	---	---	---	0.9996	---	---	
	F-PFO	1	0.5987	---	---	---	---	---	11.24	---	
	F-PSO	2	1.2166	---	---	---	---	---	---	270.09	
	F-PNO	1.50	0.9206	---	---	---	---	---	---	50.94	

	organic molecules		etched		pseudo n^{th} order								2020)
NF/RO	Treatment of waste water	Permeate	Aromatic polyamide composite	<60	Normalized intermediate blocking	$J = \frac{J_{pu} \cdot \exp(k \cdot J_{pu} \cdot t)}{J_{pu} + \exp(k \cdot J_{pu} \cdot t) - 1}$	0,9 910	----	----	----	----	----	(Tong <i>et al.</i> , 2020)
MF	Retention of colloidal and organic compounds	Retentate	Micro-fluidic Mimic	<600	Complete pore blocking	$J = J_0 \cdot \exp(-K_b \cdot t)$	0,9 768	----	----	----	----	----	(Debnath <i>et al.</i> , 2019)
DF	Purification of several monoclonal antibodies compounds	Rejection	Cellulose(XO HC)	<500	Cake-adsorption fouling	$CF_{cap,i} = \alpha_0 + \alpha_1 \cdot K_{C,i} + \alpha_2 \cdot K_{A,i} + \alpha_3 \cdot K_{C,i}^2$	0,8 600	----	----	----	----	----	(Goldrick <i>et al.</i> , 2017)
MF	Separation of bovine serum albumin in protein solution	Permeate	Polyethylene	<31	Cake filtration intermediate blocking	$V = \frac{1}{K_i} \cdot Ln \left(1 + \frac{K_i}{K_i \cdot J_0} \left(\sqrt{1 + 2 \cdot K_i \cdot J_0^2} - 1 \right) \right)$	1.9 982	----	----	----	----	----	(Heidari <i>et al.</i> , 2017)
MF	Separation of mixture Oil/Water	Permeate and Rejection	Polyvinylidene fluoride	<60	Intermediate blocking	$V = \frac{1}{K_i} \cdot Ln(1 + K_i \cdot J_0 \cdot t)$	0,9 896	----	----	----	----	----	(Fouladitajar <i>et al.</i> , 2013)
				<60	Genetic programming	$Y = \cos \sin \cos(\log(\sin x_1 + \sin \sin x_1) - ((\sin x_2 \cdot \cos x_2 \cdot \cos \cos x_1) + \cos \cos \cos(\sin \sin((\log x_2 \cdot \log x_1 \cdot x_1 \cdot x_1) \cdot (-\sin \log x_2 - (\cos \cos \cos(x_1 \cdot x_2) \cdot \log(x_2 \cdot \sin x_1) \cdot \cos \log \cos x_2 \cdot \cos x_2) + \sin \sin \sin x_1)) - x_1) \cdot (\cos \log x_2 - (x_1 + x_2)) - x_1) \cdot (\cos \cos((\log(\cos x_1 + \log x_1 \cdot \cos x_1)) \cdot \cos((x_2 - 2 \cdot \cos x_2 \cdot x_2))) + x_1) \cdot (\cos((\cos \log \cos x_2) \cdot (x_2 \cdot \log(x_2 \cdot \sin x_1))) \cdot x_2)) - \cos x_1)))$	0,9 999	----	----	----	----	----	

CF_{cap} is the filter capacity at pressure i ($L \cdot m^{-2}$). J is the filtrate flux ($L \cdot m^{-2} \cdot h^{-1}$). P is the pressure (Pa).

4. Conclusion

In this study, improved fractional dimensionless models have been developed from the pseudo n^{th} order equation and validated by statistical criteria to comprehensively

follow the DWRO desalination process using the dimensionless cumulative volume of alimentation, permeate and rejection. The validation of developed models was conducted using 2561 experimental data

points collected over a span of 4 years from 66 organics RO membranes.

Such as, the fractional dimensionless models with the optimal kinetic constant (n , α , k_n and k_{nf}) demonstrated an accurate result and a perfect consistency to the experimental data of DWRO desalination process. The statistical criteria were perfect with high values of R^2 (0.9975, 0.9750 and 0.980) and with lower values of AARD, RMSE, SSR and SSE for alimentation, permeate and rejection, respectively. As though, the optimal order of the fractional model has the advantage of using for universal separating kinetic via RO process.

Abbreviation

AARD	Average Absolute Relative Deviation
DF	Depth Filtration
DWRO	Dam Water Reverse Osmosis
FDE	Fractional Differential Equation
FDM	Fractional Dimensionless Models
F-PFO	Fractional Pseudo-First-Order
F-PNO	Fractional Pseudo-nth-Order
F-PSO	Fractional Pseudo-Second-Order
F-PZO	Fractional Pseudo-Zero-Order
MAE	Mean Absolute Error
MF	Microfiltration
NF	Nanofiltration
ODE	Ordinary Differential Equation
ODM	Ordinary Dimensionless Models
O-PFO	Ordinary Pseudo-First-Order
O-PNO	Ordinary Pseudo-nth -Order
O-PSO	Ordinary Pseudo-Second-Order
O-PZO	Ordinary Pseudo-Zero-Order
PNO	Pseudo nth Order
R^2	Coefficient of Determination
RMSE	Root Mean Squared Error
RO	Reverse osmosis
SSE	Sum of Squares Error
SSR	Sum of Squares Regression
TDS	Total Dissolved Salt

Declaration of Competing Interest

The authors declare that they have no known competing financial interests or personal relationships that could have appeared to influence the work reported in this paper.

Acknowledgments

Sincere appreciation is expressed to Dr. Ahmed AZIZI and Pr. Salah HANINI. In addition, thanks are extended to the water treatment services at the Antibiotic complex (SAIDAL) of Medea, (Algeria).

References

Abid M.F., Zablouk M.A. and Abid-Alameer A.M. (2012). Experimental study of dye removal from industrial wastewater by membrane technologies of reverse osmosis

and nanofiltration, *Iranian Journal of Environmental Health Science & Engineering*, **9**(1), 17–17

Adda A., Hanini S., Abbas M., and Sediri M. (2020), Novel adsorption model of filtration process in polycarbonate track-etched membrane: Comparative study, *Environmental Engineering Research*, **25**(4), 479–487.

Ahmed M.A., Amin S. and Mohamed A.A. (2023). Fouling in reverse osmosis membranes: monitoring, characterization, mitigation strategies and future directions, *Heliyon*, **9**, e14908.

Alsarayreh A.A., Al-Obaidi M.A., Al-Hroub A.M., Patel R. and Mujtaba I.M. (2020). Evaluation and minimization of energy consumption in a medium-scale reverse osmosis brackish water desalination plant, *Journal of Cleaner Production*, **248**, 119220.

Azizi A., Abouda L., Hanini S. and Moussaoui M. (2022). Empirical correlation with dimensionless parameters for following the kinetic separation performance via reverse osmosis desalination process of groundwater, *Global NEST Journal*, **24**(4), 638–661.

Bchiti M., Igouzal M., El-Ghizel S. and El Midaoui A. (2022). Modeling pore blocking of nanofiltration and reverse osmosis membranes during NaCl removal, *Bulgarian Chemical Communications*, **54**(3), 199–204.

Blanchard G., Maunaye M., and Martin G. (1984). Removal of heavy metals from waters by means of natural zeolites, *Water Research*, **18**(12), 501–1507.

Coker A.K. (1995). Fortran Programs for Chemical Process Design, Analysis, and Simulation- CHAPTER 1 - Numerical Computation, 1-102, *Gulf Publishing Company, Houston, Texas, USA*.

De Souza Matias G., Bissaro C.A., Matos Jorge L.M. and Rossoni D.F. (2019), The fractional calculus in studies on drying: A new kinetic semi-empirical model for drying, *The Journal of Food Process Engineering*, **42**(1), e12955.

Debnath N., Kumar A., Thundat T. and Sadrzadeh M. (2019). Investigating fouling at the pore-scale using a microfluidic membrane mimic filtration system, *Scientific Reports*, **9**, 10587.

Dimitriou E., Boutikos P., Mohamed E.S., Koziel S. and Papadakis G. (2017). Theoretical performance prediction of a reverse osmosis desalination membrane element under variable operating conditions, *Desalination*, **419**, 70–78.

El-Gazar E.F., Zahra W.K., Hassan H. and Rabia S.I. (2021). Fractional modeling for enhancing the thermal performance of conventional solar still using hybrid nanofluid: energy and exergy analysis, *Desalination*, **503**, 114847.

Feria-Díaz J.J., Correa-Mahecha F., López-Méndez M.C., Rodríguez-Miranda J.P. and Barrera-Rojas J. (2021). Recent desalination technologies by hybridization and integration with reverse osmosis: a review, *Water*, **13**(10), 1369.

Fouladitajar A., Ashtiani F. Z., Okhovat A. and Dabir B. (2013). Membrane fouling in microfiltration of oil-in-water emulsions, a comparison between constant pressure blocking laws and genetic programming (GP) model, *Desalination*, **329**, 41–49.

Friesen V.C., Leitões D.P., Gonçalves G., Lenzi E.K. and Lenzi M.K. (2015). Modeling heavy metal sorption kinetics using fractional calculus, *Hindawi-Mathematical Problems in Engineering*, **11**, 1–8.

- Fritzmann C., Löwenberg J., Wintgens T. and Melin T. (2007). State-of-the-art of reverse osmosis desalination, *Desalination*, **216**(1-3), 1–76.
- Glaser J. (1998). The early history of reverse osmosis membrane development, *Desalination*, **117**, 297–309.
- Goldrick S., Joseph A., Mollet M., Turner R., Gruber D., Farid S.S. and Titchener-Hooker N.J. (2017). Predicting performance of constant flow depth filtration using constant pressure filtration data, *Journal of Membrane Sciences*, **531**, 138–147.
- Heidari S., Etemadi H. and Yegani R. (2021). A comprehensive analysis of membrane fouling in microfiltration of complex linear macromolecules based on theoretical modeling and FESEM images, *Journal of Chemical Technology & Biotechnology*, **96**(2), 360–373.
- Heidari S., Jafarzadeh Y., Samarin M. S. and Yegani R. (2017). Study on the fouling behavior of HDPE/PE-g-MA/EVA blend membrane fabricated via thermally induced phase separation method, *Polyolefins Journal*, **4**(2), 235–251.
- Hermans P.H. and Bredée H.L. (1935). Zur kenntnis der filtrationsgesetze, *Recueil des Travaux Chimiques des Pays-Bas*, **54**(9), 680–700.
- Ho C.C. and Zydney A.L. (2000). A combined pore blockage and cake filtration model for protein fouling during microfiltration, *Journal of Colloid and Interface Science*, **232**(2), 389–399.
- Jamal K., Khan M.A. and Kamil M. (2004). Mathematical modeling of reverse osmosis systems, *Desalination*, **160**(1), 29–42.
- Jouyban A., Chan H.K., and Foster N.R. (2002). Mathematical representation of solute solubility in supercritical carbon dioxide using empirical expressions, *The Journal of supercritical fluids*, **24** (1), 19–35.
- Kashchenko N.M. and Nikitin M.A. (2014). Simulation of anomalous-diffusion effects for drainage systems, *Mathematical Models and Computer Simulations*, **6**, 337–341.
- Kumar D., Singh J., Tanwar K. and Baleanu D. (2019). A new fractional exothermic reactions model having constant heat source in porous media with power, exponential and Mittag-Leffler laws, *International Journal of Heat and Mass Transfer*, **138**, 1222–1227.
- Lagergren S. (1898). Zur Theorie der sogenannten Adsorption gelöster Stoffe, *Bihang till Kongl. Svenskavetenskaps-akademiens handlingar*, **24**(4), 1–39.
- Lee S. and Elimelech M. (2006). Relating organic fouling of reverse osmosis membranes to intermolecular adhesion forces, *Environmental Science & Technology*, **40**(3), 980–987.
- Lemus-Mondaca R., Nuñez H., Jaques A., Ramírez C. and Simpson R. (2021). The anomalous diffusion model based on a fractional calculus approach applied to describe the rehydration process of dried vegetal food matrices, *The Journal of Food Process Engineering*, **44**(9), e13773.
- Leyva-Ramos R., Rivera-Utrilla J., Medellín-Castillo N.A. and Sanchez-Polo M. (2010). Kinetic modeling of fluoride adsorption from aqueous solution onto bone char, *Chemical Engineering Journal*, **158**, 458–467.
- Mahdad A., Laidi M., Hanini S., Hentabli M. and Amrane A. (2021a). A Grey wolf optimizer-based fractional calculus in studies on solar drying, *Kemija u industriji*, **70**(1-2), 39–47.
- Mahdad A., Laidi M., Hanini S., Hentabli M. and Benhelal M. (2021b). Modelling the drying kinetics of apple (Golab Variety): fractional calculus vs semi-empirical models, *Kemija u industriji*, **70**(5-6), 251–262.
- Mesli C., Laidi M., Hanini S., Adda A., Moussaoui M. and Hentabli M. (2022). Fractional calculus-based modelling of membrane filtration, *Kemija u Industriji*, **71**(1-2), 1–7.
- Mirza I.A., Akram M.S., Shah N.A., Akhtar S. and Muneer M. (2021). Study of one dimensional contaminant transport in soils using fractional calculus, *Mathematical Methods in the Applied Sciences*, **44**(8), 6839–6856.
- Morais W.A., de Almeida A.L.P., Pereira M.R. and Fonseca J.L.C. (2008). Equilibrium and kinetic analysis of methyl orange sorption on chitosan spheres, *Carbohydrate Research*, **343**, 2489–2493.
- Morais W.A., Fernandes A.L.P., Dantas T.N.C., Pereira M.R. and Fonseca J.L.C. (2007). Sorption studies of a model anionic dye on crosslinked chitosan, *Colloids and Surfaces A: Physicochem. Eng. Aspects*, **310**, 20–31.
- Nikan O., Machado J.A.T., Golbabai A. and Nikazad T. (2020). Numerical approach for modeling fractal mobile/immobile transport model in porous and fractured media, *International Communications in Heat and Mass Transfer*, **111**, 104443.
- Obembe A.D., Abu-Khamsin S.A., Hossain M.E. and Mustapha K. (2018). Analysis of subdiffusion in disordered and fractured media using a Grünwald-Letnikov fractional calculus model, *Computational Geosciences*, **22**(5), 1231–1250.
- Padrino J.C. (2017). On the self-similar, early-time, anomalous diffusion in random networks-Approach by fractional calculus, *International Communications in Heat and Mass Transfer*, **89**, 134–138.
- Qrenawi L.I. and Abuhabib A.A. (2020). A review on sources, types, mechanisms, characteristics, impacts and control strategies of fouling in RO membrane systems, *Desalination and Water Treatment*, **208**, 4369.
- Ramírez C., Astorga V., Nuñez H., Jaques A. and Simpson R. (2017). Anomalous diffusion based on fractional calculus approach applied to drying analysis of apple slices: The effects of relative humidity and temperature, *The Journal of Food Process Engineering*, **40**(5), e12549.
- Ruth B.F., Montillar G.H. and Montonna R.E. (1933). Studies in filtration - I. Critical analysis of filtration theory, *Industrial and Engineering Chemistry*, **25**(1), 76–82.
- Soleimani R., Dehaghani A.H.S., Shoushtari N.A., Yaghoubi P. and Bahadori A. (2018). Toward an intelligent approach for predicting surface tension of binary mixtures containing ionic liquids, *Korean Journal of Chemical Engineering*, **35**(7), 1556–1569.
- Tien C., Ramarao B.V. and Yasarli R. (2014). A blocking model for membrane filtration, *Chemical Engineering Science*, **111**, 421–431.
- Tong X., Wu Y.H., Wang Y.H., Bai Y., Zhao X.H., Luo L.W., Mao Y., Ikuno N. and Hu H.Y. (2020). Simulating and predicting the flux change of reverse osmosis membranes over time during wastewater reclamation caused by organic fouling, *Environment International*, **140**, 105744.
- Tseng R.L., Wu P.H., Wu F.C. and Juang R.S. (2014). A convenient method to determine kinetic parameters of adsorption processes by nonlinear regression of pseudo-nth-order equation, *Chemical Engineering Journal*, **237**, 153–161.

- Xu H., Xiao K., Yu J., Huang B., Wang X., Liang S., Wei C., Wen X. and Huang X. (2020). A Simple method to identify the dominant fouling mechanisms during membrane filtration based on piecewise multiple linear regressions, *Membrane*, **10**(8), 171.
- Zhai S., Gui D., Huang P. and Feng X. (2015). A novel high-order ADI method for 3D fractional convection–diffusion equations, *International Communications in Heat and Mass Transfer*, **66**, 212–217.
- Özer A. (2007). Removal of Pb(II) ions from aqueous solutions by sulphuric acid-treated wheat bran, *Journal of Hazardous Materials*, **141**, 753–761.

UNCORRECTED PROOFS